

Peroxy acetyl nitrate (PAN) measurements at northern mid-latitude mountain sites in April: A constraint on continental source-receptor relationships

Arlene M. Fiore^{1,2}, Emily V. Fischer³, George P. Milly², Shubha Pandey Deolal⁴, Oliver Wild⁵, Dan Jaffe^{6,7}, Johannes Staehelin⁴, Olivia E. Clifton^{1,2}, Dan Bergmann⁸, William Collins⁹, Frank Dentener¹⁰, Ruth M. Doherty¹¹, Bryan N. Duncan¹², Bernd Fischer¹³, Stefan Gilge^{14,15}, Peter G. Hess¹⁶, Larry W. Horowitz¹⁷, Alexandru Lupu^{18,19}, Ian MacKenzie¹¹, Rokjin Park²⁰, Ludwig Ries²¹, Michael G. Sanderson²², Martin G. Schultz²³, Drew T. Shindell²⁴, Martin Steinbacher²⁵, David S. Stevenson¹¹, Sophie Szopa²⁶, Christoph Zellweger²⁵, Guang Zeng²⁷

¹Department of Earth and Environmental Science, Columbia University, Palisades, NY, 10964, U.S.A.

²Lamont-Doherty Earth Observatory of Columbia University, Palisades, NY, 10964, U.S.A.

³Department of Atmospheric Science, Colorado State University, Fort Collins, CO, 80521, U.S.A.

⁴Institute for Atmospheric and Climate Science, ETH Zürich, Switzerland

⁵Lancaster Environment Centre, Lancaster University, Lancaster, LA1 4YQ, UK

⁶School of STEM, University of Washington, Bothell, WA, 98011, U.S.A.

⁷Department of Atmospheric Science, University of Washington, Seattle, WA, 98195, U.S.A.

⁸Lawrence Livermore National Laboratory, Livermore, CA, 94550, U.S.A.

⁹Department of Meteorology, University of Reading, Reading, RG6 6BB, UK

¹⁰European Commission, Joint Research Centre, Ispra, I-21027, Italy

¹¹School of GeoSciences, The University of Edinburgh, Edinburgh, EH9 3FF, UK

¹²Atmospheric Chemistry and Dynamics Laboratory, NASA GSFC, Greenbelt, MD 20720, U.S.A.

¹³Federal Environment Agency (UBA), Schauinsland, 79254, Germany

¹⁴Meteorological Observatory Hohenpeissenberg, German Meteorological Service (DWD), Hohenpeissenberg, DE

¹⁵now at DWD, Research Center Human Biometeorology, Freiburg, DE

¹⁶Department of Biological and Environmental Engineering, Cornell University, Ithaca, NY, 14853, U.S.A.

¹⁷Geophysical Fluid Dynamics Laboratory, National Oceanic and Atmospheric Administration, Princeton, NJ, 08540, U.S.A.

¹⁸Centre for Research in Earth and Space Science, York University, Toronto, M3J 1P3, Canada

¹⁹now at Air Quality Research Division, Environment and Climate Change Canada, Toronto, M3H 5T4, Canada

²⁰School of Earth and Environmental Sciences, Seoul National University, Seoul, 08826, Republic of Korea

²¹II4.5.7, German Environment Agency (UBA), Zugspitze, 82475, Germany

²²Met Office, Exeter, EX1 3PB, UK.

²³Jülich Supercomputing Centre, Forschungszentrum Jülich, 52425 Jülich, Germany

²⁴Nicholas School of the Environment, Duke University, Durham, NC, 27708, U.S.A.

²⁵Laboratory for Air Pollution / Environmental Technology, Empa – Swiss Federal Laboratories for Materials Science and Technology, Dübendorf, CH-8600, Switzerland

²⁶Laboratoire des Sciences du Climat et de l'Environnement, Institut Pierre Simon Laplace, CEA/CNRS/UVSQ, Gif sur Yvette, France

²⁷National Institute of Water and Atmospheric Research, Wellington, 6021, New Zealand

Correspondence to: Arlene M. Fiore (amfiore@ldeo.columbia.edu)

Abstract. Abundance-based model evaluations with observations provide critical tests for the simulated mean state in models of intercontinental pollution transport, and under certain conditions may also offer

48 constraints on model responses to emission changes. We compile multi-year measurements of peroxy
49 acetyl nitrate (PAN) available from five mountaintop sites and apply them in a proof of concept approach
50 that exploits an ensemble of global chemical transport models (HTAP1) to identify an observational
51 “emergent constraint”. In April, when the signal from anthropogenic emissions on PAN is strongest,
52 simulated PAN at northern mid-latitude mountaintops correlates strongly with PAN source-receptor
53 relationships (the response to 20% reductions in precursor emissions within northern mid-latitude
54 continents; hereafter, SRRs). This finding implies that PAN measurements can provide constraints on PAN
55 SRRs by limiting the SRR range to that spanned by the subset of models simulating PAN within the
56 observed range. In some cases, regional anthropogenic volatile organic compound (AVOC) emissions,
57 tracers of transport from different source regions, and SRRs for ozone also correlate with PAN SRRs.
58 Given the large observed interannual variability in the limited available datasets, establishing strong
59 constraints will require matching meteorology in the models to the PAN measurements. Application of this
60 evaluation approach to the chemistry-climate models used to project changes in atmospheric composition
61 will require routine, long-term mountaintop PAN measurements to discern both the climatological SRR
62 signal and its inter-annual variability.

63 **1 Introduction**

64 Peroxy acetyl nitrate (PAN) is produced alongside ozone (O_3) from photochemical reactions involving
65 precursor emissions of nitrogen oxides (NO_x) and non-methane volatile organic compounds (VOC). Once
66 ventilated from a source region to free troposphere where it is more stable at colder temperatures, PAN can
67 be efficiently transported throughout the hemisphere (Singh, 1987; Singh and Hanst, 1981). When a PAN-
68 containing free tropospheric air mass subsides, PAN thermally decomposes to release NO_x and can thus
69 facilitate O_3 formation far downwind (Wild et al., 1996; Schultz et al., 1999; Jaeglé et al., 2003;
70 Kotchenruther et al., 2001a; Hudman et al., 2004). Both PAN and O_3 distributions over any northern mid-
71 latitude region reflect the combined influence of production from sources within the region and transport
72 from outside that region. At northern mid-latitudes, the intercontinental influence from anthropogenic
73 emissions on surface O_3 levels is largest during spring (e.g., HTAP 2010) and occurs via at least two
74 pathways: (1) O_3 can be produced within a polluted continental boundary layer, ventilated to the free
75 troposphere and efficiently transported to other continents; and (2) O_3 can be produced in transit from the
76 export and subsequent chemical evolution of PAN and other precursors. Below, we examine the extent to
77 which springtime PAN observations at northern mid-latitude mountaintop sites can be used to constrain the
78 spread in multi-model estimates of source-receptor relationships (SRRs), where the sources are continental-
79 scale regions and the receptors are the mountaintop sites, for both PAN and O_3 .

80

81 Observations during several aircraft field campaigns in the Eastern Pacific and at mountain top sites in the
82 Western U.S. and North Atlantic document efficient O_3 production in the lower troposphere following
83 subsidence of PAN-containing air masses (Fischer et al., 2010; Heald et al., 2003; Hudman et al., 2004;

84 Kotchenruther et al., 2001a,b; Val Martin et al., 2008; Zhang et al., 2008). When PAN decomposes in low-
85 NO_x regions of the atmosphere, the NO_x released can produce O₃ up to eight times more efficiently than in
86 polluted (high-NO_x) regions (Liang et al., 1998; Liu et al., 1987) and thus increase global O₃ abundances
87 (Moxim et al., 1996; Wang and Jacob, 1998), as O₃ formation is NO_x-limited in most of the free
88 troposphere (Chameides et al., 1992). The lifetime of PAN against thermal decomposition is about 1 hour
89 at 20°C, and it approximately doubles for every 4°C decrease in temperature, leading to a lifetime of at
90 least a month in the mid-troposphere during spring. This strong temperature dependence implies that a
91 warmer climate will decrease PAN export from polluted continental boundary layers, although a rise in
92 temperature-sensitive biogenic precursor emissions may temper this response (e.g. Doherty et al., 2013).
93 Future projections of atmospheric composition under global change scenarios will thus benefit from a
94 thorough understanding of the role PAN plays in transporting oxidized reactive nitrogen and thereby
95 altering ozone production throughout the troposphere

96

97 To better distinguish among disparate estimates for intercontinental O₃ transport in the published literature,
98 the Task Force on Hemispheric Transport of Air Pollution (HTAP) organized an international global
99 modelling study, referred to here as HTAP1. The HTAP1 study identified a factor of two range across
100 individual model estimates of surface O₃ response to changes in anthropogenic precursor emissions from
101 continental-scale, northern mid-latitude source regions (HTAP 2007; Fiore et al., 2009; HTAP 2010; Wild
102 et al. 2012). The HTAP1 models do not distinguish between intercontinental O₃ transport occurring due to
103 O₃ produced from PAN chemistry versus direct transport of O₃ formed in a remote boundary layer, but
104 other work indicates that both pathways contribute. Jaegle et al. (2003) find that 28% of the O₃ in the
105 Pacific Northwest free troposphere between 0-6 km is associated with PAN-to-NO_x conversion, consistent
106 with Jiang et al. (2016) who found that PAN produced from East Asian emissions and exported to the free
107 troposphere contributes 35% and 25% in spring and summer, respectively, to the free tropospheric O₃
108 abundance over western North America. Over East Asia, Lin et al. (2010) found that the export of PAN
109 produced from European anthropogenic emission changes and subsequent downwind O₃ formation
110 contributed 20% of the spatially averaged response of surface O₃ levels, and up to 50% of the O₃ response
111 at mountain sites.

112

113 In addition to the direct influence of PAN on intercontinental O₃ transport, PAN may serve as a sensitive
114 diagnostic of model uncertainties in O₃ production chemistry and transport (Emmerson and Evans, 2009;
115 Kuhn et al., 1998). Prior analysis of measurements and global model simulations suggests that PAN
116 abundances at high altitude sites may be more sensitive than O₃ itself to changes in precursor emissions
117 (Fiore et al., 2011; Fischer et al., 2011; Jaffe et al., 2007). We interpret this stronger sensitivity of PAN
118 than O₃ to changes in precursor emissions as reflecting buffering of O₃ by compensating changes to O₃
119 losses, whereas PAN loss pathways are far less sensitive to changes in precursor emissions. PAN loss
120 pathways include thermal decomposition (which dominates below approximately 7 km); photolysis in the

121 upper troposphere; and dry deposition within the boundary layer (Kirchner et al., 1999; Roberts, 2007;
122 Turnipseed et al., 2006). All of the HTAP1 models include PAN formation, but the chemical mechanisms
123 and kinetic rate coefficients differ, with likely implications for long-range transport (Emmerson and Evans,
124 2009; Knote et al., 2015). A prior multi-model study found that even with the same emissions, PAN differs
125 widely across models, reflecting differences in simulated photochemistry (Emmons et al., 2015). While the
126 absence of direct emissions and its low background make PAN a useful tracer of photochemistry, we note
127 that O₃ typically responds more strongly to changes in NO_x emissions, while PAN responds more strongly
128 to changes in VOC emissions in many regions (Fischer et al., 2014; see their Figure 4).

129

130 A challenge in discriminating among model estimates of O₃ produced from different source regions is the
131 lack of direct observational constraints on SRRs. For example, Fiore et al. (2009) did not find any
132 relationship across models between their biases against surface O₃ observations and the strength of their
133 response to emission changes. In the absence of an observable quantity to constrain these relationships,
134 one approach is to identify an “emergent constraint” (Borodina et al., 2017), whereby a non-observable
135 quantity correlates strongly across a multi-model ensemble with an observed variable. The inter-model
136 range of the non-observable quantity is then narrowed by limiting it to the range encompassed by the
137 models closest to the observed variable. This approach has gained traction for narrowing the spread across
138 future climate projections (e.g., Hall and Qu, 2006; Cox et al. 2018). In light of its role as a proxy for ozone
139 formation chemistry, its direct role in facilitating intercontinental ozone transport, and the large signature of
140 PAN originating in the European boundary layer during spring found at Jungfraujoch (Pandey Deolal et al.,
141 2013, 2014), we hypothesize that PAN measurements may offer much-needed constraints for
142 discriminating across model estimates of intercontinental transport of PAN, and possibly O₃. The number
143 of models contributing to the HTAP1 study, which was designed to maximize comparability across
144 individual model estimates of ozone responses to changes in precursor emissions within northern mid-
145 latitude continental-scale source regions, offers an opportunity to evaluate this hypothesis.

146

147 We describe the HTAP1 model simulations, mountaintop measurements and our strategy to sample the
148 models at these sites (Section 2) before illustrating our rationale for selecting the month of April to quantify
149 the range of multi-model PAN distributions and PAN measurements at northern mid-latitude mountain sites
150 (Section 3). We then borrow from the “emergent constraint” approach in climate science to show that
151 correlations between simulated total PAN and SRRs for PAN are sufficiently strong as to permit PAN
152 measurements at mountaintop sites (one in each of the three major mid-latitude source regions) to narrow
153 the wide inter-model spread in estimates of PAN origin (Section 4). We further examine inter-model
154 relationships between the simulated PAN SRRs at these three mountaintop sites and regional precursor
155 emissions, and with a proxy for model transport (Section 5). Finally, we assess the relationship between
156 PAN and O₃ SRRs (Section 6) and conclude with a summary and recommendations for future work based
157 on our proof of concept analysis (Section 7).

158 **2. Approach**

159 **2.1 HTAP1 model simulations**

160 We use monthly mean PAN mixing ratios for the year 2001 simulated by fourteen global chemistry
161 transport models (Table 1); the temporal resolution for three-dimensional chemical fields archived from the
162 HTAP1 models is limited to monthly. We use four HTAP1 Source-Receptor (SR) simulations (Table 2): a
163 base case (SR1) and three perturbation simulations in which anthropogenic O₃ precursor emissions (NO_x,
164 VOC, carbon monoxide and aerosols) are reduced simultaneously by 20% within East Asia (SR6EA),
165 Europe and northern Africa (SR6EU), and North America (SR6NA). We calculate PAN SRRs by
166 differencing the perturbation and base simulations (SR1-SR6XX), where XX refers to the region in which
167 emissions of PAN precursors were decreased by 20%.

168

169 Of the models in Table 1, eleven used 2001 meteorological fields. Two models are chemistry-transport
170 models coupled directly to a general circulation model forced by observed sea surface temperatures
171 (STOC-HadAM3 and STOCHEM) and one model incorporates chemistry directly into a general circulation
172 model (UM-CAM). We include these models as our evaluation compiles PAN measurements across
173 several years (Section 2.2). The individual model specifications and emissions are described in Tables 1
174 and 2 of Fiore et al. (2009). For HTAP1, each model used its own emissions inventories (see Table A1 of
175 Fiore et al., 2009); Fiore et al. (2009) provide emission totals within each HTAP1 source region for all
176 (their Table A2) and anthropogenic (their Table A3) emissions of NO_x, NMVOC, and CO. The relative
177 inter-model spread in regional anthropogenic emissions is smallest for NO_x emissions in EU and NA
178 (<10%) and largest for VOC from EU (58%) (Fiore et al. 2009).

179

180 To separate the role of inter-model differences in transport from the combined impacts of inter-model
181 differences in emissions and chemistry on simulated PAN at the mountaintop sites, we analyze an
182 additional set of idealized tracer simulations available from eleven models (COfromXX in Table 1, where
183 XX is the source region). In these simulations, a set of tagged carbon monoxide-like tracers are emitted,
184 each from a single HTAP1 source region with a 50-day lifetime, and with identical emissions across
185 models. Biomass burning emissions for the CO tracers are from GFED (van der Werf et al., 2006; 2010)
186 and other emissions are from the RETRO project (Schultz et al., 2007; 2008). We refer to these tracers as
187 “COfromEA”, “COfromNA”, and “COfromEU”, which denote the tracers emitted from EA, NA, EU,
188 respectively (Table 2; see also Doherty et al., 2013 and Shindell et al., 2008).

189 **2.2 Multi-year PAN measurements at mountaintop sites and model sampling**

190 To evaluate the HTAP1 models, we compiled April mean climatologies of lower tropospheric PAN
191 measurements from northern mid-latitude mountain observatories (Table 3). Given the large interannual

192 variability in PAN abundances, we require at least two years of observations in April. PAN observations
193 from Mount Bachelor (U.S.A.), Jungfrauoch (Switzerland), and Zugspitze (Schneefernerhaus),
194 Hohenpeissenberg, and Schauinsland (all in Germany) meet these criteria. Taken together, these
195 mountaintop measurements span 15 years, from 1995 to 2010 (Table 3), although only one site
196 (Schauinsland) overlaps with the HTAP1 simulation year of 2001.

197

198 PAN was measured at all five mountain sites using gas chromatography with electron capture detection
199 (ECD). A custom system using a Shimadzu Mini-2 ECD was employed at Mount Bachelor (Fischer et al.,
200 2010). The commercially available Meteorologie Consult (GmbH) system was used at the European sites
201 (Zellweger et al., 2000). Calibrations generate PAN from the photolysis of excess acetone and NO in air
202 (Warneck and Zerbach, 1992; Volz-Thomas et al., 2002). Reported detection limits are ~20 ppt for PAN
203 measurements at Mount Bachelor, and ~50 ppt for the European sites, with total uncertainties of <10%
204 (Fischer et al., 2010; Zellweger et al., 2003).

205

206 We include all available data at these sites without filtering for upslope winds or any other criteria. At
207 Mount Bachelor, the cleanest of the 5 mountaintop sites (Supplemental Figure 1), Fischer et al. (2010) have
208 shown that PAN mixing ratios are not primarily controlled by diurnal wind patterns, which lead to
209 variations an order of magnitude smaller than the total observed range in measured PAN. When
210 measurements fall below the detection limit, we include half of the detection limit. This assumption should
211 not affect our conclusions as mountaintop sites generally sample free tropospheric air at night (e.g., Weiss-
212 Penzias et al., 2004) but PAN values below the detection limit typically occur due to deposition in a
213 shallow nocturnal boundary layer.

214

215 For comparison with the observations, we sample each model on its native grid (Table 1) at the horizontal
216 grid cell containing the latitude and longitude of each mountain site. Orography at these mountain sites is
217 poorly resolved at the relatively coarse HTAP1 model horizontal resolutions. This mismatch requires us to
218 apply some approximations for vertical sampling. We convert the station altitude to an approximate
219 pressure level by assuming a mean tropospheric temperature of 260 K, and a corresponding atmospheric
220 scale height of 7.6 km. We then use monthly mean pressure fields from each model to linearly interpolate
221 PAN based on the pressures of the two model grid cells that vertically bound the station pressure. While
222 different sampling strategies may alter the exact value of simulated PAN and its comparison to
223 observations, our primary interest is in the inter-model differences. Although the Zugspitze and
224 Hohenpeissenberg sites fall within the same horizontal grid cell in the HTAP1 models, the station altitudes
225 differ, so we consider the two sites separately.

226

227 Given that we seek constraints on intercontinental transport from the three major mid-latitude source
228 regions, we conduct a more in-depth analysis at the highest altitude European site (Jungfrauoch), the most

229 likely of the available sites to measure PAN transported between continents in the free troposphere, as well
230 as at Mount Bachelor in North America. At Jungfraujoch, we also evaluate SRRs in the models with an
231 estimate of PAN originating in the European boundary layer based on an analysis of 20-day back
232 trajectories (Pandey Deolal et al., 2013). We conduct a proof of concept analysis at Mount Waliguan in
233 Asia (36.28°N, 100.90°E, 3816 m) to assess the potential for future PAN measurements at this site to
234 narrow the inter-model range in SRRs. Short-term measurements have previously been collected at this site
235 (Xue et al., 2011). While aircraft and satellite observations have advanced the understanding of the
236 chemistry and dynamics of individual PAN plumes using models that archived higher temporal frequency
237 chemical fields (e.g., Alvarado et al., 2010; Payne et al., 2014; Emmons et al., 2015), their limited temporal
238 coverage is not well suited for comparison with the HTAP1 monthly mean PAN mixing ratios.

239 **3. Modeled and measured lower tropospheric PAN at northern mid-latitudes in April**

240 Our goal is to assess the potential for mountaintop PAN measurements to discriminate among model
241 estimates of PAN and O₃ produced by regional anthropogenic emissions and transported to the
242 mountaintop sites. We thus focus our analysis on April when measured PAN reaches its seasonal maximum
243 (Penkett and Brice, 1986; Singh and Salas, 1989; Bottenheim et al., 1994; Schmitt and Volz-Thomas, 2004;
244 Supplemental Figure 1) and when the HTAP1 models indicate that the production of PAN from the EA,
245 EU, and NA source regions dominates total simulated PAN (Figure 1). April thus offers the strongest
246 possible signal of the influence of anthropogenic emissions from these three northern mid-latitude source
247 regions in the mountaintop measurements.

248

249 Figure 2 shows the spatial distribution of the HTAP1 model ensemble mean PAN mixing ratios at 650 hPa
250 (~3 km), the level sampled by the highest altitude sites on which we focus the majority of our analysis.
251 PAN mixing ratios in April generally increase with latitude, as expected from the strong thermal
252 dependence of the PAN lifetime, although some of the highest mixing ratios are simulated over the Asian
253 source region. The multi-model spread in lower tropospheric PAN, represented by the coefficient of
254 variation (standard deviation over the 14 models divided by the model ensemble mean) is within ±45%
255 across much of the northern hemisphere (Figure 2). The large inter-model spread over much of Europe in
256 Figure 2b implies that observational constraints in this region would be particularly valuable.

257

258 Observed and modelled PAN mixing ratios at the northern mid-latitude mountain sites are compared in
259 Figure 3; see Supplemental Figure 1 for a comparison extended throughout the year). We consider the
260 measured range across years to bound the “plausible” portion of the wide range in simulated total PAN
261 across the models. The multi-model mean falls in the range of the measurements at four of the sites, but is
262 higher than observed in any year at Mount Bachelor. The model rankings show some consistency across
263 the different sites, suggesting systematic model differences that can be narrowed with a limited set of
264 observational constraints, especially for models that rank similarly across the sites on all three continents

265 (Figure 3). For example, CAMCHEM and GEMAQ are consistently at the higher end of the range while
266 GISS-PUCCINI and LLNL-IMPACT are at the low end. The two models falling closest to the observed
267 2001 value at Schauinsland (MOZECH and MOZARTGFDL) fall into the observed range at either Mount
268 Bachelor or Jungfraujoch; we analyze these two sites further in the following sections.

269

270 The longest observational dataset at Schauinsland varies by over a factor of three across years, consistent
271 with large inter-annual variability found in prior analyses at mountaintop sites (Zellweger et al., 2003;
272 Fischer et al., 2011; Pandey Deolal et al. 2013, 2014). All but one of the models (LLNL-IMPACT) fall
273 within the wide range of observed inter-annual variability at Schauinsland, underscoring the tenuous nature
274 of conclusions regarding model performance drawn from short observational records unless the modelled
275 and observed meteorological years match. Future work to coordinate consistent time periods between
276 measurements and models would provide tighter constraints than are possible with our proof-of-concept
277 analysis described in the following sections.

278 **4. Exploring emergent constraints on model SRRs from measured total PAN**

279 The range of the PAN SRRs across the HTAP1 models at Jungfraujoch, Mount Bachelor, and Mount
280 Waliguan is wide for all three source regions, spanning a factor of five or more in several cases (Figure 4).
281 The key to a successful emergent constraint analysis is for this range in inter-model PAN SRRs, our
282 unobservable quantity, to correlate with the total PAN simulated at the mountaintop site, our observable
283 variable. The strongest correlations emerge for PAN originating in the region where the mountain is
284 located, but some intercontinental SRR pairs also show significant correlations ($p \leq 0.05$) with total
285 simulated PAN (Figure 4).

286

287 We illustrate here how PAN measurements can be used to narrow the inter-model range in the SRR pairs.
288 For the sites with significant correlations, the range across years (i.e., red vertical lines in Figure 4) bound
289 the April mean values observed at Jungfraujoch and Mount Bachelor. The models falling in this range are
290 highlighted in red. We select these models to narrow the range in SRRs, indicated by the red horizontal
291 dashed lines extending from the bounding models (red symbols) to the ordinate axis. Figure 4 shows that
292 the constraint from total measured PAN narrows the inter-model range in SRRs for PAN by at least half,
293 revealing some models as outliers. Other models simulate SRRs within the observationally constrained
294 range (between the dashed red horizontal lines) despite falling outside the observed range for total PAN,
295 possibly indicating a role for inter-model differences in non-anthropogenic sources of PAN or in the
296 relative contributions from the individual mid-latitude source regions, which we investigate further in the
297 next section. Given the year-to-year variability in total PAN, stronger constraints could be placed in future
298 work where the model meteorology corresponds to the same year as the measurements.

299

300 At Jungfraujoch, we additionally consider PAN SRRs for the EU source region with those estimated
301 previously by back-trajectory analysis (Pandey Deolal, 2013). While Pandey Deolal (2013) also attribute
302 trajectories to NA and EA, fewer than 15% and 4% of trajectories are attributed to those regions as
303 compared to 25-50% from EU (range across years; see Figure 1 of Pandey Deolal (2013)). Combining
304 these low frequencies with the inevitable growth in uncertainty as trajectories lengthen, we have the most
305 confidence in the Pandey Deolal (2013) estimates for the EU region. The horizontal blue dashed lines
306 indicate the bounds obtained from this trajectory-based approach to estimating PAN from EU. The models
307 falling in these bounds overlap with those constrained by the total PAN measurements, lending some
308 confidence that these two independent approaches (one using total PAN and the correlated inter-model
309 spread in SRRs; the other using back-trajectories to estimate SRRs) yield useful constraints on the
310 influence of the EU source region on PAN measured at Jungfraujoch.

311

312 We note that for consistency with the model SRRs in Figure 4, which are the responses to 20% emission
313 reductions in the source region, we divide the Pandey Deolal (2013) EU SRRs by five to scale back from
314 their estimated “full contribution” (100%). This linear scaling of the PAN response between 20% and
315 100% may incur errors due to non-linear chemistry. With an additional simulation in which the
316 FRSGUCI model sets European anthropogenic emissions of NO_x, CO and VOC to zero (a 100%
317 perturbation), we estimate this error to be ~10%. For intercontinental regions, this error reduces to <3%.
318 Earlier work shows that the smaller non-linearity in PAN for intercontinental versus regional source-
319 receptor pairs also holds for ozone (Fiore et al., 2009; Wu et al., 2009; Wild et al., 2012), and demonstrates
320 approximate linearity between the simulated tropospheric ozone burden and ±50% of present-day global
321 NO_x emissions (Stevenson et al., 2006).

322 **5. Factors contributing to the inter-model range in PAN SRRs**

323 We investigate the role of inter-model differences in regional emissions of PAN precursors versus transport
324 in contributing to inter-model differences in the PAN response to continental-scale emission changes at the
325 three mountaintop sites shown in Figure 4. At each site, we examine the correlation across models between
326 simulated PAN SRRs and regional anthropogenic emissions of VOC (AVOC; Figure 5) or NO_x (ANO_x).
327 The relationships for the EA SRRs are not significant, even at Mount Waliguan. We find, however, that the
328 inter-model range in regional AVOC emissions explains as much as 64% of the variation in PAN attributed
329 to EU emissions, and at least 25% of the variance in PAN attributed to the NA region (Figure 5). In
330 contrast to AVOC, we find little relationship between the range in simulated PAN source-receptor
331 relationships at the mountain sites and the model spread in regional ANO_x emissions. Fischer et al. (2014)
332 have previously shown that PAN abundances respond more strongly to changes in emissions of VOC than
333 of NO_x. Our analysis supports that earlier finding and furthermore highlights a key role for model
334 differences in regional AVOC emissions in contributing to the inter-model range in PAN SRRs.

335

336 Differences in model transport (e.g., Arnold et al., 2015; Orbe et al., 2017) may also contribute to the inter-
337 model differences in PAN SRRs. Our analysis of the HTAP1 idealized CO tracers, however, reveals little
338 correlation between inter-model differences in these idealized tracers (which have identical regional
339 emissions and lifetimes applied in all of the models) and in the PAN SRRs sampled at these sites. Although
340 we do not find any clear overall correlation, differences in the idealized CO tracers explain some of the
341 scatter in Figure 5. For example, at Jungfraujoch for EU AVOC emissions of 22 Tg C a⁻¹, the lowest model
342 (GISS-PUCCINI) has one of the smallest values for the CO_{fromEU} tracer, whereas the highest model
343 (STOC-HadAM3) has the largest value of CO_{fromEU}.

344

345 In light of the dependence of inter-model differences in PAN attributed to EU and NA during April and the
346 corresponding regional AVOC emissions, we illustrate how one could extend our emergent constraints in
347 Figure 4 (horizontal dashed red lines) to the regional AVOC emission estimates shown in Figure 5. A
348 major caveat underlying this analysis is the mis-match between meteorological years for the models and
349 measurements as discussed above, and the underlying assumption that the relationships in Figure 5 can
350 exclusively be attributed to differences in the AVOC emissions (as opposed to chemistry or transport).
351 The observationally-constrained SRRs between PAN from NA and total PAN measured at Jungfraujoch
352 and Mount Bachelor can be used to narrow the range of NA AVOC emissions to 12-18 Tg C a⁻¹ (the low
353 end is ruled out by the constraint imposed by PAN from NA at Jungfraujoch; the high end is ruled out by
354 PAN from NA at Mount Bachelor). Similarly, the range for EU AVOC emissions would narrow to 16-25
355 Tg C a⁻¹.

356

357 We consider next the importance that various models ascribe to a given source region relative to another
358 source region. We first correlate the ratios of PAN from two different source regions with the total PAN
359 simulated by the individual models in April. We find little relationship, with the exception of Mount
360 Bachelor, where, intriguingly, the observational constraint implies that more PAN originating from EA
361 should be present at Mount Bachelor than PAN originating from NA (Figure 6a). We interpret this as
362 indicating that models with higher total PAN at Mount Bachelor are overestimating North American
363 influence at this mountain site sampling free tropospheric air. This interpretation is supported by the
364 idealized CO tracer simulations (with identical regional emissions and the same lifetime applied in all the
365 models), which suggest that some of the variance in the ratio of PAN from NA versus EA at Mount
366 Bachelor is due to different transport from the two regions (Figure 6b). We emphasize that these transport
367 differences do not simply reflect the use of different meteorology to drive the CTMs (Figure 6b).

368

369 We examine systematically the relative importance of emissions within the source region where the
370 measurement site is located versus the upwind intercontinental source region on PAN at the three
371 mountaintop sites, by comparing NA:EA at Mount Bachelor, EU:NA at Jungfraujoch, and EA:EU at Mount
372 Waliguan (Supplemental Figure 2). At Mount Bachelor, the HTAP1 multi-model mean SRRs from NA,

373 EA, and EU, are roughly equal in April (Figure 1). The differences across the HTAP models in the relative
374 importance of the NA:EA source regions on PAN (which range from about 0.5 to 2.5) correlate roughly
375 equally with the ratio of the NA:EA transport tracers and with the ratio of the NA:EA AVOC emissions;
376 we find no relationship with the ratio of the NA:EA ANO_x emissions (Figure 6b and Supplemental Figure 2
377 left column; Spearman rank correlation coefficient (r) = 0.6 for both cases). At Jungfraujoch, the HTAP1
378 multi-model mean attributes much of the PAN to emissions from the EU and NA source regions during
379 April (Figure 1). The ratio of PAN attributed to EU versus NA at Jungfraujoch, however, varies from
380 approximately 0.5 to 2 across the individual HTAP1 models (Supplemental Figure 2). In contrast to our
381 findings at Mount Bachelor, this ratio at Jungfraujoch depends most strongly on the ratio of ANO_x
382 emissions in the EU to NA regions (r = 0.6), and more weakly on the ratio of EU:NA AVOC emissions (r =
383 0.5; Supplemental Figure 2). The correlation is even weaker between the ratio of PAN SRRs for these two
384 regions with inter-model differences in transport as diagnosed with the CO tracers from EU versus NA (r =
385 0.4). At Mount Waliguan, the strongest relationship is found for the ratio of AVOC emissions (r = 0.5;
386 Supplemental Figure 2).

387

388 We repeat this correlation analysis of inter-model differences in ratios of ANO_x emissions, AVOC
389 emissions, or the idealized tracers of transport from a region, but for the ratio of PAN SRRs from two
390 intercontinental regions. At Mount Bachelor, the EU and EA source regions contribute similar amounts to
391 multi-model mean PAN during April (Figure 1). Across the individual models, however, the ratio of the EU
392 to EA source region on PAN at Mount Bachelor varies from less than half to a factor of two (Supplemental
393 Figure 3). We find that the ratio of PAN attributed to the EU versus EA source regions at Mount Bachelor
394 correlates strongly across the models with the ratio of the anthropogenic volatile organic compound
395 (AVOC) emissions in the respective source regions (r = 0.8; Supplemental Figure 3). In contrast, the ratio
396 of EU:EA anthropogenic emission influence on PAN at Mount Bachelor shows little correlation with the
397 respective regional NO_x emissions used in the models, or with the differences in the simulated transport
398 tracers (r =0.3 for both cases). As at Mount Bachelor, the model spread in the contribution to total simulated
399 PAN from the EA versus NA source regions at both Jungfraujoch and Mount Waliguan depend most on the
400 regional AVOC ratios (r = 0.8 and 0.6, respectively; Supplemental Figure 3), with little correlation with
401 inter-model differences in NA:EA ANO_x emissions. Some correlation also emerges between the NA:EA
402 source-receptor relationships for PAN and the NA:EA transport tracers (r = 0.6 at both sites; Supplemental
403 Figure 3). Finally, we do not find any obvious link between PAN SRRs and the choice of meteorological
404 fields (the individual symbols in Supplemental Figures 2 and 3).

405 **6. Linking PAN and O₃ SRRs**

406 We address here the extent to which observational constraints on PAN SRRs might also serve to narrow the
407 range of uncertainty in the inter-model spread in intercontinental SRRs for O₃ (e.g., Fiore et al., 2009). We
408 expect some commonality between the sensitivity of PAN and O₃ to changes in precursor emissions

409 because (1) both species are produced from chemical reactions involving NO_x and VOC, and (2) PAN
410 serves as a NO_x reservoir, which upon decomposition releases NO_x that can then produce O₃ far downwind
411 of the region where the PAN (and O₃) precursors were originally emitted. Furthermore, earlier analysis of
412 HTAP1 ozone continental-scale SRRs also identified a correlation with the model AVOC emissions,
413 particularly over the EU (Fiore et al., 2009).

414

415 We assess the extent to which the inter-model range in source region influence on mountaintop PAN levels
416 in April is relevant for interpreting O₃ SRRs by correlating PAN and O₃ SRRs at the three mountaintop
417 sites (Figure 7). Relationships vary across the individual source-receptor pairs, with the inter-model
418 variability in PAN explaining 16-60% of the inter-model differences in O₃ at the mountain sites. The
419 strongest relationships occur for the influence of regional sources on at Mount Bachelor (from NA) and
420 Jungfrauoch (EU). At Mount Waliguan, the EU and EA source-receptor relationships for PAN and O₃ are
421 of similar strength ($r = 0.7$). Intercontinental source-receptor pairs for O₃ and PAN at Mount Bachelor and
422 Mount Waliguan are also significant to within 90%, with variability in the PAN attributed to
423 intercontinental source regions explaining 25-35% and 30-45%, respectively, of the variability in the
424 corresponding O₃ source-receptor relationship.

425

426 We expand the correlation analysis of ozone and PAN SRRs from the free troposphere sampled at the
427 mountaintop sites to large-scale SRRs in surface air over the HTAP1 continental regions. Of the significant
428 relationships in Figure 7 ($p < 0.10$), 6 out of 7 also show significant relationships in Figure 8. We infer that
429 conclusions drawn from a limited number of mountaintop sites regarding PAN SRRs and their relationship
430 to ozone SRRs are relevant, at least according to the models, on much broader scales.

431

432 We repeat the analysis in Figure 5 but for O₃ to consider the influence of the three source regions on the
433 three mountaintop sites (nine total source-receptor pairs), but find little relationship between the model
434 spread in the simulated O₃ SRRs and in the magnitude of the regional AVOC or ANO_x emissions. Model
435 differences in transport as diagnosed by the idealized regional CO tracers correlates more with O₃ SRRs
436 than for PAN for all source-receptor pairs, though the correlations remains weak except for COfromEU and
437 O₃ SRRs at Jungfrauoch. Overall, this analysis supports earlier findings that PAN is more sensitive to
438 changes in emissions (and subsequent chemistry), particularly for VOC precursors, than O₃.

439

440 The correlations between SRRs for PAN and O₃ could reflect a role for PAN transport in contributing to O₃
441 production over the receptor region, or may instead reflect co-production of PAN and O₃ from oxidation of
442 regional precursor emissions followed by transport in the same air mass. In the latter case, PAN is serving
443 as a proxy for O₃ transport whereas in the former case, PAN is serving as the actual pathway by which O₃ is
444 transported. We do not have model diagnostics that allow us to distinguish between these two roles for
445 PAN. The correlations between PAN and O₃ SRRs, however, suggest that long-term PAN measurements

446 contain signals relevant for constraining the relative importance of regional vs. intercontinental emissions
447 on both PAN and O₃. We examine the strength of these signals by correlating the O₃ SRRs at each site
448 with total PAN as simulated at each site. Relationships are far weaker than for the PAN SRRs and total
449 PAN shown in Figure 4, but correlations do emerge between total PAN at Jungfraujoch for O₃ from EU
450 ($r=0.67$; $p=0.03$) and at Mount Bachelor for O₃ from NA ($r=0.61$; $p=0.04$; Supplemental Figure 4).

451 **7. Conclusions and recommendations**

452 Our proof of concept approach applies the HTAP1 multi-model ensemble to identify a strong inter-model
453 correlation between PAN source-receptor relationships (SRRs; defined as the difference in simulations with
454 20% emission reductions separately within each of the northern mid-latitude continents) and simulated total
455 PAN at mountaintop sites during April. Our findings imply promise for developing “emergent constraints”
456 (e.g., Hall and Qu, 2006; Borodina et al., 2017; Cox et al., 2018) from mountaintop PAN measurements to
457 narrow uncertainty in wide-ranging model estimates of PAN SRRs, quantities that are not directly
458 observable yet relevant to air quality policy (e.g., HTAP 2010). Inter-model correlations of the responses
459 of PAN versus O₃ to perturbations in regional anthropogenic emissions (Figures 7 and 8) imply that
460 constraints on PAN SRRs are relevant for lowering uncertainty in O₃ SRR estimates. This connection
461 between PAN and O₃ likely reflects the dual role of PAN as both a pathway for O₃ transport (by producing
462 O₃ upon its decomposition following transport), and as a proxy for O₃ transport (as it is produced alongside
463 O₃ in the polluted continental boundary layer).

464
465 Establishing the strongest constraints possible on simulated SRRs for PAN and O₃ will require (1)
466 measurements and simulations with chemical transport models that coincide, and (2) a sufficiently long
467 measurement record to build a climatology suitable for evaluating chemistry-climate models that generate
468 their own meteorology. To tackle the first requirement, we recommend a coordinated field campaign and
469 multi-model study during April with simultaneous PAN measurements at high altitude mountaintop sites
470 (e.g., Jungfraujoch, Mount Bachelor, and Mount Waliguan). To address the second requirement, we
471 recommend long-term coordinated measurements for assessing chemistry-climate models and for testing
472 the representation of inter-annual variability in chemical transport models (and chemistry-climate models
473 nudged to observed meteorology). Repeated sampling for the month of April may be sufficient to provide
474 constraints on model responses to changes in anthropogenic emissions. Long-term measurements could
475 directly observe the response of PAN to emission changes over time, as long as inter-annual variability in
476 meteorology is taken into account. As a next step, monthly mean PAN archived from newer multi-model
477 ensembles whose simulations span recent decades (e.g., Chemistry-Climate Model Initiative (CCMI),
478 HTAP Phase 2 (HTAP2) simulations, and the anticipated AerChemMIP simulations) could be evaluated
479 with the multi-year records in Table 3; comparison to Schauinsland may offer a particularly useful testbed.
480

481 We identified only five multi-year datasets at mountain sites, four of which are located near each other in
482 Europe, and only one of which continues at present (Schauinsland). Our analysis suggests that
483 measurements at Mount Waliguan would provide constraints on PAN SRRs, particularly for PAN
484 originating in EA (Figure 4). Additional work could systematically examine over 60 stations at altitudes
485 above 2500 m in the Tropospheric Ozone Assessment Report (TOAR) database (Schultz et al., 2017).
486 Adding PAN to the suite of species measured routinely aboard commercial aircraft (Eckstein et al., 2017;
487 Petzold et al., 2015) would provide PAN distributions across much of the northern mid-latitude free
488 troposphere for evaluating models (and PAN satellite products).

489

490 We recommend archival of daily model fields for future applications of this multi-model emergent
491 constraint approach to SRRs. Access to daily model fields permits (1) a more rigorous process-oriented
492 evaluation of specific events (e.g., Fischer et al., 2010; Alvarado et al., 2010; Arnold et al., 2015), and (2)
493 comparison with satellite-derived tropospheric PAN columns, which show promise for documenting PAN
494 distributions, particularly in the upper troposphere, and their temporal variability and spatial patterns across
495 the globe (e.g., Fadnavis et al., 2014; Jiang et al., 2016; Payne et al., 2014; 2017; Zhu et al., 2015; 2017).
496 We also suggest archiving daily tracers tagged by emission region to isolate the role of model differences in
497 transport during individual events. In addition, Lin et al. (2017) have demonstrated that applying a filtering
498 technique based on daily idealized CO regional tracers can better isolate free tropospheric air from surface
499 air masses when comparing coarse resolution models with high altitude measurements.

500

501 By focusing on April, our analysis largely minimizes complexities introduced by inter-model differences in
502 biogenic, fire, and lightning sources that further complicate disentangling summertime discrepancies in
503 simulated PAN and O₃ (e.g., Arnold et al., 2015; Emmons et al., 2015) and restricts inter-model differences
504 to those associated with anthropogenic emissions and the subsequent chemistry and transport.
505 Nevertheless, we find a wide range in inter-model SRR relationships that reflects uncertainties in
506 emissions and different model representations of VOC chemistry, including PAN yields from VOCs
507 (Figure 5; Emmerson and Evans, 2009; Fischer et al., 2014; Arnold et al., 2015; Emmons et al., 2015;
508 Knote et al., 2015). Future multi-model efforts could seek to parse separately the influence of differences
509 in total anthropogenic VOC emissions, the mix of emitted VOC species and their reactivity, and the
510 chemical production of PAN and O₃. Documenting these aspects of model configuration would help to
511 establish benchmarks for inter-model differences in simulated total PAN, O₃, and their SRRs, against which
512 future model simulations (and multi-model ensembles) can be assessed.

513

514 Strong observational constraints, such as may be possible with the approach we outline here, are needed to
515 build confidence in model responses of PAN to climate change (e.g., by changing temperature and weather-
516 sensitive precursor emissions) and the resulting influence on atmospheric ozone and oxidizing capacity
517 (e.g., Doherty et al., 2013). Changes in meteorology and biomass burning (Fischer et al., 2011; Zhu et al.,

518 2015) such as those driven by ENSO (Koumoutsaris et al., 2008), as well as biogenic and lightning sources
519 (Payne et al., 2017) vary from year to year and are expected to change as climate warms. Long-term,
520 springtime observations of PAN in the free troposphere could be a keystone measurement for testing
521 models projecting future atmospheric composition under scenarios with changes in both precursor
522 emissions and climate.

523 **Acknowledgments**

524 We thank Mathew Evans (York University, UK) and Terry Keating (U.S. EPA) for useful discussions.
525 AMF and BND acknowledge NASA MAP (NNX14AM38G). DSS acknowledges NERC (grants
526 NE/K001329/1 and NE/N003411/1) and the ARCHER UK National Supercomputing Service
527 (<http://www.archer.ac.uk>). Data for the Mt. Bachelor Observatory are archived and available at the
528 University of Washington data archive:
529 <https://digital.lib.washington.edu/researchworks/browse?type=subject&value=Mt.+Bachelor+Observatory>.
530 The PAN data for the European Mountain sites is archived by the World Data Centre for Greenhouse Gases
531 (<http://ds.data.jma.go.jp/gmd/wdcgg/>). Upon publication, the data used to generate the figures will be
532 placed in a CSU digital repository that we have already established for this manuscript
533 (<https://hdl.handle.net/10217/185610>). This is Lamont contribution number...

534 **References**

- 535 Alvarado, M. J., and 35 others: Nitrogen oxides and PAN in plumes from boreal fires during ARCTAS-B
536 and their impact on ozone: an integrated analysis of aircraft and satellite observations, *Atmos. Chem.*
537 *Phys.*, 10, 9739–9760, doi:10.5194/acp-10-9739-2010, 2010.
- 538 Arnold, S. R., Emmons, L. K., Monks, S. A., Law, K. S., Ridley, D. A., Turquety, S., Tilmes, S., Thomas,
539 J. L., Bouarar, I., Flemming, J., Huijnen, V., Mao, J., Duncan, B. N., Steenrod, S., Yoshida, Y.,
540 Langner, J., and Long, Y.: Biomass burning influence on high-latitude tropospheric ozone and reactive
541 nitrogen in summer 2008: a multi-model analysis based on POLMIP simulations, *Atmos. Chem. Phys.*,
542 15, 6047–6068, <https://doi.org/10.5194/acp-15-6047-2015>, 2015.
- 543 Balzani Lööv, J. M., S. Henne, G. Legreid, J. Staehelin, S. Reimann, A. S. H. Prévôt, M. Steinbacher, and
544 M. K. Vollmer: Estimation of background concentrations of trace gases at the Swiss Alpine site
545 Jungfraujoch (3580 m asl), *J. Geophys. Res.*, 113, D22305, doi:[10.1029/2007JD009751](https://doi.org/10.1029/2007JD009751), 2008.
- 546 Borodina, A., Fischer, E. M., R. Knutti, Emergent Constraints in Climate Projections: A Case Study of
547 Changes in High-Latitude Temperature Variability, *Journal of Climate*, [https://doi.org/10.1175/JCLI-](https://doi.org/10.1175/JCLI-D-16-0662.1)
548 [D-16-0662.1](https://doi.org/10.1175/JCLI-D-16-0662.1), 2017.
- 549 Bottenheim, J. W., Sirois, A., Brice, K. A., and Gallant, A. J.: Five years of continuous observations of
550 PAN and ozone at a rural location in eastern Canada, *Journal of Geophysical Research: Atmospheres*,
551 99, 5333–5352, 10.1029/93JD02716, 1994.

552 Carpenter, L. J., Green, T. J., Mills, G. P., Bauguitte, S., Penkett, S. A., Zanis, P., Schuepbach, E.,
553 Schmidbauer, N., Monks, P. S., Zellweger, C.: Oxidized nitrogen and ozone production efficiencies in
554 the springtime free troposphere over the Alps, *J. Geophys. Res.*, 105, D11, 14,547-14,559, 2000.

555 Chameides, W. L., Fehsenfeld, F. C., Rodgers, M. O., Cardelino, C., Martinez, J., Parrish, D., Lonnerman,
556 W., Lawson, D. R., Rasmussen, R. A., Zimmerman, P., Greenberg, J., Middleton, P., and Wang, T.:
557 Ozone precursor relationships in the ambient atmosphere, *Journal of Geophysical Research*, 97, 6037-
558 6055, 1992.

559 Cox, P. M., Huntingford, C., and Williamson, M. S., Emergent constraint on equilibrium climate
560 sensitivity from global temperature variability: *Nature*, 553, 319, 10.1038/nature25450, 2018.

561 Doherty, R. M., et al.: Impacts of climate change on surface ozone and intercontinental ozone pollution: A
562 multi-model study, *J. Geophys. Res. Atmos.*, 118, doi:10.1002/jgrd.50266, 2013.

563 Eckstein, J., Ruhnke, R., Zahn, A., Neumaier, M., Kirner, O., and Braesicke, P.: An assessment of the
564 climatological representativeness of IAGOS-CARIBIC trace gas measurements using EMAC model
565 simulations, *Atmos. Chem. Phys.*, 17, 2775-2794, <https://doi.org/10.5194/acp-17-2775-2017>, 2017.

566 Emmerson, K. M., and Evans, M. J.: Comparison of tropospheric gas-phase chemistry schemes for use
567 within global models, *Atmos. Chem. Phys.*, 9, 1831-1845, 10.5194/acp-9-1831-2009, 2009.

568 Emmons, L. K., Arnold, S. R., Monks, S. A., Huijnen, V., Tilmes, S., Law, K. S., Thomas, J. L., Raut, J.-
569 C., Bouarar, I., Turquety, S., Long, Y., Duncan, B., Steenrod, S., Strode, S., Flemming, J., Mao, J.,
570 Langner, J., Thompson, A. M., Tarasick, D., Apel, E. C., Blake, D. R., Cohen, R. C., Dibb, J., Diskin,
571 G. S., Fried, A., Hall, S. R., Huey, L. G., Weinheimer, A. J., Wisthaler, A., Mikoviny, T., Nowak, J.,
572 Peischl, J., Roberts, J. M., Ryerson, T., Warneke, C., and Helmig, D.: The POLARCAT Model
573 Intercomparison Project (POLMIP): overview and evaluation with observations, *Atmos. Chem. Phys.*,
574 15, 6721-6744, <https://doi.org/10.5194/acp-15-6721-2015>, 2015.

575 Fadnavis, S., Schultz, M. G., Semeniuk, K., Mahajan, A. S., Pozzoli, L., Sonbawne, S., Ghude, S. D.,
576 Kiefer, M., and Eckert, E.: Trends in peroxyacetyl nitrate (PAN) in the upper troposphere and lower
577 stratosphere over southern Asia during the summer monsoon season: regional impacts, *Atmos. Chem.*
578 *Phys.*, 14, 12725-12743, <https://doi.org/10.5194/acp-14-12725-2014>, 2014.

579 Fiore, A. M., Dentener, F. J., Wild, O., Cuvelier, C., Schultz, M. G., Hess, P., Textor, C., Schulz, M.,
580 Doherty, R. M., Horowitz, L. W., MacKenzie, I. A., Sanderson, M. G., Shindell, D. T., Stevenson, D.
581 S., Szopa, S., Van Dingenen, R., Zeng, G., Atherton, C., Bergmann, D., Bey, I., Carmichael, G.,
582 Collins, W. J., Duncan, B. N., Faluvegi, G., Folberth, G., Gauss, M., Gong, S., Hauglustaine, D.,
583 Holloway, T., Isaksen, I. S. A., Jacob, D. J., Jonson, J. E., Kaminski, J. W., Keating, T. J., Lupu, A.,
584 Marmer, E., Montanaro, V., Park, R. J., Pitari, G., Pringle, K. J., Pyle, J. A., Schroeder, S., Vivanco,
585 M. G., Wind, P., Wojcik, G., Wu, S., and Zuber, A.: Multimodel estimates of intercontinental source-
586 receptor relationships for ozone pollution, *J. Geophys. Res.*, 114, D04301, 10.1029/2008jd010816,
587 2009.

588 Fiore, A. M., Levy II, H., and Jaffe, D. A.: North American isoprene influence on intercontinental ozone
589 pollution, *Atmos. Chem. Phys.*, 11, 1697-1710, 10.5194/acp-11-1697-2011, 2011.

590 Fischer, E. V., Jaffe, D. A., Reidmiller, D. R., and Jaegle, L.: Meteorological controls on observed
591 peroxyacetyl nitrate (PAN) at Mount Bachelor during the spring of 2008, *Journal of Geophysical*
592 *Research*, 115 doi: 10.1029/2009JD0012776, 2010.

593 Fischer, E. V., Jaffe, D. A., and Weatherhead, E. C.: Free tropospheric peroxyacetyl nitrate (PAN) and
594 ozone at Mount Bachelor: potential causes of variability and timescale for trend detection, *Atmos.*
595 *Chem. Phys.*, 11, 5641-5654, 10.5194/acp-11-5641-2011, 2011.

596 Fischer, E. V., Jacob, D. J., Yantosca, R. M., Sulprizio, M. P., Millet, D. B., Mao, J., Paulot, F., Singh, H.
597 B., Roiger, A., Ries, L., Talbot, R. W., Dzepina, K., and Pandey Deolal, S.: Atmospheric peroxyacetyl
598 nitrate (PAN): a global budget and source attribution, *Atmos. Chem. Phys.*, 14, 2679-2698,
599 10.5194/acp-14-2679-2014, 2014.

600 Gilge, S., Plass-Dülmer, C., Fricke, W., Kaiser, A., Ries, L., Buchmann, B., and Steinbacher, M.: Ozone,
601 carbon monoxide and nitrogen oxides time series at four alpine GAW mountain stations in central
602 Europe, *Atmos. Chem. Phys.*, 10, 12295-12316, 10.5194/acp-10-12295-2010, 2010.

603 Hall, A., and Qu, X., Using the current seasonal cycle to constrain snow albedo feedback in future climate
604 change: *Geophys. Res. Lett.*, 33, L03502, doi:10.1029/2005GL025127, 2006.

605 Heald, C. L., Jacob, D. J., Fiore, A. M., Emmons, L. K., Gille, J. C., Deeter, M. N., Warner, J., Edwards,
606 D. P., Crawford, J. H., Hamlin, A. J., Sachse, G. W., Browell, E. V., Avery, M. A., Vay, S. A.,
607 Westberg, D. J., Blake, D. R., Singh, H. B., Sandholm, S. T., Talbot, R. W., and Fuelberg, H. E.: Asian
608 outflow and trans-Pacific transport of carbon monoxide and ozone pollution: An integrated satellite,
609 aircraft, and model perspective, *J. Geophys. Res.*, 108, 4804, 10.1029/2003jd003507, 2003.

610 HTAP: Task Force on Hemispheric Transport of Air Pollution 2007 Interim Report, United Nations
611 Economic Commission for Europe, New York and Geneva, 2007.

612 HTAP: HEMISPHERIC TRANSPORT OF AIR POLLUTION 2010 PART A: OZONE AND
613 PARTICULATE MATTER, Air Pollution Studies No. 17, UNITED NATIONS, New York, 2010.

614 Hudman, R. C., Jacob, D. J., Cooper, O. R., Evans, M. J., Heald, C. L., Park, R. J., Fehsenfeld, F., Flocke,
615 F., Holloway, J., Hübler, G., Kita, K., Koike, M., Kondo, Y., Neuman, A., Nowak, J., Oltmans, S.,
616 Parrish, D., Roberts, J. M., and Ryerson, T.: Ozone production in transpacific Asian pollution plumes
617 and implications for ozone air quality in California, *J. Geophys. Res.*, 109, D23S10,
618 10.1029/2004jd004974, 2004.

619 Jaeglé, L., Jaffe, D. A., Price, H. U., Weiss-Penzias, P., Palmer, P. I., Evans, M. J., Jacob, D. J., and Bey,
620 I.: Sources and budgets for CO and O₃ in the northeastern Pacific during the spring of 2001: Results
621 from the PHOBEA-II Experiment, *Journal of Geophysical Research*, 108, doi:10.1029/2002JD003121,
622 2003.

623 Jaffe, D., Thornton, J., Wolfe, G., Reidmiller, D., Fischer, E. V., Jacob, D. J., Cohen, R., Singh, H.,
624 Weinheimer, A., and Flocke, F.: Can we Detect an Influence over North America From Increasing
625 Asian NO_x Emissions?, *EOS Trans. AGU*, 88(52), Fall Meet. Suppl., Abstract A51E-04, 2007.

626 Jiang, Z., Worden, J. R., Payne, V. H., Zhu, L., Fischer, E., Walker, T., and Jones, D. B. A.: Ozone export
627 from East Asia: The role of PAN, *Journal of Geophysical Research: Atmospheres*, 121, 6555-6563,
628 10.1002/2016JD024952, 2016.

629 Kirchner, F., Mayer-Figge, A., Zabel, F., and Becker, K. H.: Thermal stability of peroxy nitrates,
630 *International Journal of Chemical Kinetics*, 31, 127-144, 1999.

631 Knote, C., Tuccella, P., Curci, G., Emmons, L., Orlando, J. J., Madronich, S., Baro, R., Jimenez-Guerrero,
632 P., Luecken, D., Hogrefe, C., Forkel, R., Werhahn, J., Hirtl, M., Perez, J., San Jose, R., Giordano, L.,
633 Brunner, D., Yahya, K., Zhang, Y.: Influence of the choice of gas-phase mechanism on predictions of
634 key gaseous pollutants during the AQMEII phase-2 intercomparison, *Atmos. Environ.*, 115, 553-568,
635 2015.

636 Kotchenruther, R. A., Jaffe, D. A., and Jaeglé, L.: Ozone photochemistry and the role of PAN in the
637 springtime northeastern Pacific Troposphere: Results from the PHOBEA Campaign. *J. Geophys. Res.*,
638 106, 28731-28741, 2001a.

639 Kotchenruther, R. A., Jaffe, D. A., Beine, H. J., Anderson, T., Bottenheim, J. W., Harris, J. M., Blake, D.,
640 and Schmitt, R.: Observations of ozone and related species in the Northeast Pacific during the
641 PHOBEA Campaigns: 2. Airborne observations. *J. Geophys. Res.*, 106, 7463-7483, 2001b (corrected
642 Table 1 published in Vol. 106 (D17), p.20507).

643 Koumoutsaris, S., Bey, I., Generoso, S., and Thouret, V.: Influence of El Niño-Southern Oscillation on the
644 interannual variability of tropospheric ozone in the northern midlatitudes, *J. Geophys. Res.*, 113,
645 D19301, 10.1029/2007jd009753, 2008.

646 Kuhn, M., Builtjes, P. J. H., Poppe, D., Simpson, D., Stockwell, W. R., Andersson-Sköld, Y., Baart, A.,
647 Das, M., Fiedler, F., Hov, Ø., Kirchner, F., Makar, P. A., Milford, J. B., Roemer, M. G. M., Ruhnke,
648 R., Strand, A., Vogel, B., and Vogel, H.: Intercomparison of the gas-phase chemistry in several
649 chemistry and transport models, *Atmospheric Environment*, 32, 693-709, 1998.

650 Liang, J., Horowitz, L. W., Jacob, D. J., Wang, Y., Fiore, A. M., Logan, J. A., Gardner, G. M., and
651 Munger, J. W.: Seasonal variations of reactive nitrogen species and ozone over the United States and
652 export fluxes to the global atmosphere, *Journal of Geophysical Research*, 103, 13,435-413,450, 1998.

653 Lin, M., Horowitz, L. W., Payton, R., Fiore, A. M., and Tonnesen, G.: US surface ozone trends and
654 extremes from 1980 to 2014: quantifying the roles of rising Asian emissions, domestic controls,
655 wildfires, and climate, *Atmos. Chem. Phys.*, 17, 2943-2970, <https://doi.org/10.5194/acp-17-2943-2017>,
656 2017.

657 Lin, M., Holloway, T., Carmichael, G. R., and Fiore, A. M.: Quantifying pollution inflow and outflow
658 over East Asia in spring with regional and global models, *Atmos. Chem. Phys.*, 10, 4221-4239,
659 10.5194/acp-10-4221-2010, 2010.

660 Liu, S. C., Trainer, M., Fehsenfeld, F. C., Parrish, D. D., Williams, E. J., Fahey, D. W., Hubler, G., and
661 Murphy, P. C.: Ozone production in the Rural Troposphere and the Implications for Regional and
662 Global Ozone Distributions, *Journal of Geophysical Research*, 92, 4191-4207, 1987.

663 Moxim, W. J., Levy, H., II, and Kasibhatla, P. S.: Simulated global tropospheric PAN: Its transport and
664 impact on NO_x, *J. Geophys. Res.*, 101, 12621-12638, 10.1029/96jd00338, 1996.

665 Naja, M., H. Akimoto, and J. Staehelin: Ozone in background and photochemically aged air over central
666 Europe: Analysis of long-term ozonesonde data from Hohenpeissenberg and Payerne, *J. Geophys.*
667 *Res.*, 108, 4063, doi:[10.1029/2002JD002477](https://doi.org/10.1029/2002JD002477), D2, 2003.

668 Orbe, C., D. W. Waugh, H. Yang, J.-F. Lamarque, S. Tilmes, and D. E. Kinnison (2017), Tropospheric
669 transport differences between models using the same large-scale meteorological fields, *Geophys. Res.*
670 *Let.*, 44, 1068–1078, doi:10.1002/2016GL071339.

671 Pandey Deolal, S., Henne, S., Ries, L., Gilge, S., Weers, U., Steinbacher, M., Staehelin, J., and Peter, T.:
672 Analysis of elevated springtime levels of Peroxyacetyl nitrate (PAN) at the high Alpine research sites
673 Jungfraujoch and Zugspitze, *Atmos. Chem. Phys.*, 14, 12553-12571, 10.5194/acp-14-12553-2014,
674 2014.

675 Pandey Deolal, S., Staehelin, J., Brunner, D., Cui, J., Steinbacher, M., Zellweger, C., Henne, S., and
676 Vollmer, M. K.: Transport of PAN and NO_y from different source regions to the Swiss high alpine site
677 Jungfraujoch, *Atmospheric Environment*, 64, 103-115,
678 <https://doi.org/10.1016/j.atmosenv.2012.08.021>, 2013.

679 Payne, V. H., Alvarado, M. J., Cady-Pereira, K. E., Worden, J. R., Kulawik, S. S., and Fischer, E. V.:
680 Satellite observations of peroxyacetyl nitrate from the Aura Tropospheric Emission Spectrometer,
681 *Atmos. Meas. Tech.*, 7, 3737-3749, 10.5194/amt-7-3737-2014, 2014.

682 Payne, V. H., Fischer, E. V., Worden, J. R., Jiang, Z., Zhu, L., Kurosu, T. P., and Kulawik, S. S.: Spatial
683 variability in tropospheric peroxyacetyl nitrate in the tropics from infrared satellite observations in
684 2005 and 2006, *Atmos. Chem. Phys.*, 17, 6341-6351, 10.5194/acp-17-6341-2017, 2017.

685 Penkett, S. A., and Brice, K. A.: The spring maximum in photo-oxidants in the Northern Hemisphere
686 troposphere, *Nature*, 319, 655-657, 1986.

687 Petzold A., V. Thouret, C. Gerbig, A. Zahn, C.A.M. Brenninkmeijer, M. Gallagher, M. Hermann, M.
688 Pontaud, H. Ziereis, D. Boulanger, J. Marshall, P. Nédélec, H.G.J. Smit, U. Frieß, J.-M. Flaud, A.
689 Wahner, J.-P. Cammas, A. Volz-Thomas, and IAGOS Team: Global-Scale Atmosphere Monitoring by
690 In-Service Aircraft - Current Achievements and Future Prospects of the European Research
691 Infrastructure IAGOS, *Tellus-B*, 67, 28452, doi:10.3402/tellusb.v67.28452, 2015.

692 Roberts, J. M.: PAN and Related Compounds, in: *Volatile Organic Compounds in the Atmosphere*, edited
693 by: Koppmann, R., Blackwell Publishing, 500, 2007.

694 Schmitt, R., and Volz-Thomas, A.: Climatology of Ozone, PAN, CO, and NMHC in the Free Troposphere
695 Over the Southern North Atlantic, *Journal of Atmospheric Chemistry*, 28, 245-262,
696 10.1023/A:1005801515531, 1997.

697 Schultz, M. G. et al.: On the origin of tropospheric ozone and NO_x over the tropical South Pacific, *J.*
698 *Geophys. Res.*, 104, D5, 5829-5843, 1999.

699 Schultz, M., Rast, S., van het Bolscher, M., Pulles, T., Brand, R., Pereira, J., Mota, B., Spessa, A.,
700 Dalsoren, S., van Noije, T., and Szopa, S.: Emission data sets and methodologies for estimating
701 emissions, Hamburg, 2007.

702 Schultz, M. G., Heil, A., Hoelzemann, J. J., Spessa, A., Thonicke, K., Goldammer, J. G., Held, A. C.,
703 Pereira, J. M. C., and van het Bolscher, M.: Global wildland fire emissions from 1960 to 2000, *Global*
704 *Biogeochemical Cycles*, 22, GB2002, 10.1029/2007GB003031, 2008.

705 Schultz MG, Schröder S, Lyapina O, Cooper O, Galbally I, Petropavlovskikh I, et al.: Tropospheric Ozone
706 Assessment Report: Database and Metrics Data of Global Surface Ozone Observations, *Elem Sci*
707 *Anth.*, 5, 58, DOI: <http://doi.org/10.1525/elementa.244>, 2017.

708 Shindell, D. T., Chin, M., Dentener, F., Doherty, R. M., Faluvegi, G., Fiore, A. M., Hess, P., Koch, D. M.,
709 MacKenzie, I. A., Sanderson, M. G., Schultz, M. G., Schulz, M., Stevenson, D. S., Teich, H., Textor,
710 C., Wild, O., Bergmann, D. J., Bey, I., Bian, H., Cuvelier, C., Duncan, B. N., Folberth, G., Horowitz,
711 L. W., Jonson, J., Kaminski, J. W., Marmer, E., Park, R., Pringle, K. J., Schroeder, S., Szopa, S.,
712 Takemura, T., Zeng, G., Keating, T. J., and Zuber, A.: A multi-model assessment of pollution transport
713 to the Arctic, *Atmos. Chem. Phys.*, 8, 5353-5372, 10.5194/acp-8-5353-2008, 2008.

714 Singh, H. B.: Reactive nitrogen in the troposphere, *Environmental Science and Technology*, 21, 320-327,
715 1987.

716 Singh, H. B., and Hanst, P. L.: Peroxyacetyl nitrate (PAN) in the unpolluted atmosphere: An important
717 reservoir for nitrogen oxides, *Geophysical Research Letters*, 8, 941-944, 1981.

718 Singh, H. B., and Salas, L. J.: Measurements of peroxyacetyl nitrate (pan) and peroxypropionyl nitrate
719 (ppn) at selected urban, rural and remote sites, *Atmospheric Environment (1967)*, 23, 231-238,
720 [https://doi.org/10.1016/0004-6981\(89\)90115-7](https://doi.org/10.1016/0004-6981(89)90115-7), 1989.

721 Stevenson, D.S., et al.: Multimodel ensemble simulations of present-day and near-future tropospheric
722 ozone, *J. Geophys. Res.*, 111, D08301, doi:10.1029/2005JD006338, 2006.

723 Turnipseed, A. A., Huey, L. G., Nemitz, E., Stickel, R., Higgs, J., Tanner, D. J., Slusher, D. L., Sparks, J.
724 P., Flocke, F., and Guenther, A.: Eddy covariance fluxes of peroxyacetyl nitrates (PANs) and NO_y to a
725 coniferous forest, *Journal of Geophysical Research: Atmospheres*, 111, D09304,
726 10.1029/2005jd006631, 2006.

727 Val Martin, M., Honrath, R. E., Owen, R. C., and Lapina, K.: Large-scale impacts of anthropogenic
728 pollution and boreal wildfires on the nitrogen oxide levels over the central North Atlantic region,
729 *Journal of Geophysical Research*, 113, doi:10.1029/2007JD009689, 2008.

730 van der Werf, G. R., Randerson, J. T., Giglio, L., Collatz, G. J., Kasibhatla, P. S., and Arellano Jr, A. F.:
731 Interannual variability in global biomass burning emissions from 1997 to 2004, *Atmos. Chem. Phys.*,
732 6, 3423-3441, 10.5194/acp-6-3423-2006, 2006.

733 van der Werf, G. R., Randerson, J. T., Giglio, L., Collatz, G. J., Mu, M., Kasibhatla, P. S., Morton, D. C.,
734 DeFries, R. S., Jin, Y., and van Leeuwen, T. T.: Global fire emissions and the contribution of
735 deforestation, savanna, forest, agricultural, and peat fires (1997–2009), *Atmos. Chem. Phys.*, 10,
736 11707-11735, 10.5194/acp-10-11707-2010, 2010.

737 Volz-Thomas, A., Xueref, I., and Schmitt, R.: An automatic gas chromatograph and calibration system for
738 ambient measurements of PAN and PPN, *Environmental Science and Pollution Resources*, Special
739 Issue 4, 72-76, 2002.

740 Wang, Y., and Jacob, D. J.: Anthropogenic forcing on tropospheric ozone and OH since preindustrial
741 times, *Journal of Geophysical Research*, 103, 31,123-131,135, 1998.

742 Warneck, P., and Zerbach, T.: Synthesis of peroxyacetyl nitrate by acetone photolysis, *Environmental
743 Science and Technology*, 26, 74-79, 1992.

744 Weiss-Penzias, P., Jaffe, D. A., Jaeglé, L., and Liang, Q.: Influence of long-range-transported pollution on
745 the annual and diurnal cycles of carbon monoxide and ozone at Cheeka Peak Observatory, *Journal of
746 Geophysical Research: Atmospheres*, 109, n/a-n/a, 10.1029/2004JD004505, 2004.

747 Wild, O., Law, K., McKenna, D., Bandy, B., Penkett, S., Pyle, J.: Photochemical trajectory modeling
748 studies of the North Atlantic region during August 1993, *Journal of Geophysical Research:
749 Atmospheres*. 101, D22, p. 29269-29288, 1996.

750 Wild, O., Fiore, A. M., Shindell, D. T., Doherty, R. M., Collins, W. J., Dentener, F. J., Schultz, M. G.,
751 Gong, S., MacKenzie, I. A., Zeng, G., Hess, P., Duncan, B. N., Bergmann, D. J., Szopa, S., Jonson, J.
752 E., Keating, T. J., and Zuber, A.: Modelling future changes in surface ozone: a parameterized
753 approach, *Atmos. Chem. Phys.*, 12, 2037-2054, 10.5194/acp-12-2037-2012, 2012.

754 Wu, S., Duncan, B. N., Jacob, D. J., Fiore, A. M., and Wild, O.: Chemical nonlinearities in relating
755 intercontinental ozone pollution to anthropogenic emissions, *Geophys. Res. Lett.*, 36, L05806,
756 10.1029/2008gl036607, 2009.

757 Xue, L. K., Wang, T., Zhang, J. M., Zhang, X. C., Deliger, Poon, C. N., Ding, A. J., Zhou, X. H., Wu, W.
758 S., Tang, J., Zhang, Q. Z., and Wang, W. X.: Source of surface ozone and reactive nitrogen speciation
759 at Mount Waliguan in western China: New insights from the 2006 summer study, *J. Geophys. Res.*,
760 116, D07306, doi:10.1029/2010JD014735, 2011.

761 Zellweger, C., Ammann, M., Buchmann, B., Hofer, P., Lugauer, M., Rüttimann, R., Streit, N.,
762 Weingartner, E., and Baltensperger, U.: Summertime NO_y speciation at the Jungfrauoch, 3580 m asl,
763 Switzerland, *Journal of Geophysical Reserach*, 105, 2000.

764 Zellweger, C., Forrer, J., Hofer, P., Nyeki, S., Schwarzenbach, B., Weingartner, E., Ammann, M., and
765 Baltensperger, U.: Partitioning of reactive nitrogen (NO_y) and dependence on meteorological
766 conditions in the lower free troposphere, *Atmospheric Chemistry and Physics*, 3, 779-796, 2003.

767 Zhang, L., Jacob, D. J., Boersma, K. F., Jaffe, D. A., Olson, J. R., Bowman, K. W., Worden, J. R.,
768 Thompson, A. M., Avery, M. A., Cohen, R. C., Dibb, J. E., Flocke, F. M., Fuelberg, H. E., Huey, L.
769 G., McMillian, W. W., Singh, H. B., and Weinheimer, A. J.: Transpacific transport of ozone pollution

770 and the effect of recent Asian emission increases on air quality in North America: an integrated
771 analysis using satellite, aircraft, ozonesonde, and surface observations, *Atmospheric Chemistry and*
772 *Physics*, 8, 6117-6136, 2008.

773 Zhu, L., V. H. Payne, T. W. Walker, J. R. Worden, Z. Jiang, S. S. Kulawik, and E. V. Fischer (2017),
774 PAN in the eastern Pacific free troposphere: A satellite view of the sources, seasonality, interannual
775 variability, and timeline for trend detection, *J. Geophys. Res. Atmos.*, 122, 3614–3629,
776 doi:10.1002/2016JD025868.

777 Zhu, L., Fischer, E. V., Payne, V. H., Worden, J. R., and Jiang, Z.: TES observations of the interannual
778 variability of PAN over Northern Eurasia and the relationship to springtime fires, *Geophysical*
779 *Research Letters*, 42, 7230-7237, 10.1002/2015GL065328, 2015.

780

781

782

Table 1: Models contributing to the HTAP1 simulations (SR1, SR6xx, and COfromXX) used in this study.

Model	Resolution (lat-lon-layers)	Institute	Model contact	SR1	SR6xx	COfromxx	Plotting symbol
CAMCHEM-3311m13	2.5°x2°x30	NCAR, USA	Peter Hess	X	X	X	Filled circle
FRSGUCI-v01	2.81°x2.81°x37	Lancaster Univ., UK	Oliver Wild	X	X	X	Filled upward triangle
GEMAQ-v1p0	2°x2°x28	York Univ., Canada	Alex Lupu	X	X	X	Filled downward triangle
GEOSChem-v07	2.5°x2°x30	Harvard Univ., USA	Rokjin Park	X	X	X	Filled diamond
GISS-PUCCINI-modelE	5°x4°x23	NASA GISS, USA	Drew Shindell	X	X	X	Filled square
GMI-v02f	2.5°x2°x42	NASA GSFC, USA	Bryan Duncan	X	X	X	Open circle
LMDZ3-INCA1	3.75° x 2° x 19	CEA, France	Sophie Szopa	X	X		Open upward triangle
LLNL-IMPACT-T5a	2.5° x 2° x 48	LLNL, USA	Dan Bergmann	X			Open downward triangle
MOZARTGFDL-v2	1.88° x 1.88° x 28	NOAA GFDL, USA	Arlene Fiore	X	X	X	Open diamond
MOZECH-v16	1.88° x 1.88° x 28	FZ Julich, Germany	Martin Schultz	X	X	X	Open square
STOC-HadAM3-v01	5° x 5° x 19	University of Edinburg, UK	Ruth Doherty, David Stevenson	X	X	X	Plus sign
STOCHEM-v02	3.75° x 2.5° x 20	Met Office, Hadley Center, UK	Bill Collins, Michael	X			X

			Sanderson				
TM5-JRC-cy2- ipcc-v1	1° x 1° x 25	JRC, Italy	Frank Dentener	X	X	X	Filled right facing triangle
UM-CAM-v01	3.75° x 2.5° x 19	University of Cambridge, UK	Guang Zeng	X	X	X	Filled left facing triangle

784

785

786

787

788

789

790

791

792

793

794

795

796

797 **Table 2: Simulations from HTAP1 used in this study.**

Simulation	Description
SR1	Base case (see Section 2.1 for details)
SR6EA	SR1 but with anthropogenic emissions of all O ₃ precursors (NO _x +CO+NMVOC) and aerosols within EA decreased by 20%
SR6EU	SR1 but with 20% emissions reductions within the EU region
SR6NA	SR1 but with 20% emissions reductions within the NA region.
COfromEA	Idealized tracer simulation in which all models use identical CO emissions, emitted within the EA region, with a 50-day e-folding lifetime.
COfromEU	Same as COfromEA but for the EU region.
COfromNA	Same as COfromEA but for the NA region.

798

799

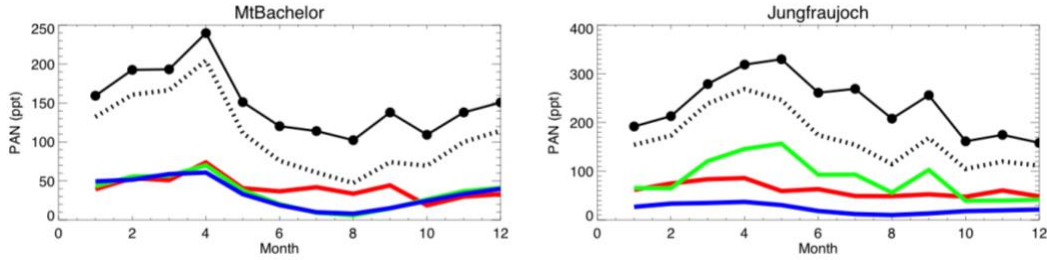
800

801

802

803 **Table 3: Mountaintop sites with multiple years of PAN observations used in this study.**

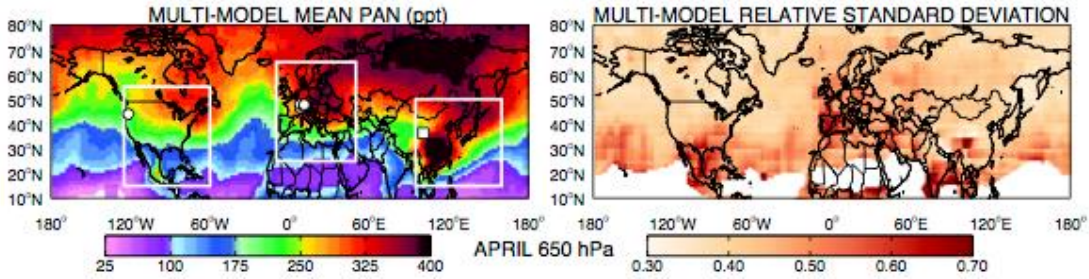
Site	Location	Elevation	Measurement Period (s)	Reference (s)
Mount Bachelor	43.979° N, 121.687° W	2763m	3 April – 18 June 2008, 30 August – 7 October 2008, 26 March – 20 May 2009, 23 March – 25 May 2010	(Fischer et al., 2010;Fischer et al., 2011)
Hohenpeissenberg	47.80° N, 11.02° E	985 m	January 2003 – December 2008	http://www.dwd.de/de/GAW (Gilge et al., 2010)
Jungfraujoch	46.55°N, 7.98°E	3580 m	April 1997 – May 1998, Aug 30 2005 – Sept 16 2005, Throughout 2005, but not continuous	(Balzani Lööv et al., 2008;Carpenter et al., 2000;Zellweger et al., 2000;Zellweger et al., 2003)
Zugspitze	47.42° N, 10.98° E	2960 m	May 2004 – December 2008	http://gaw.kishou.go.jp
Schauinsland	47.92° N, 7.92° E	1205m	January 1995 – December 2010	www.umweltbundesamt.de



804

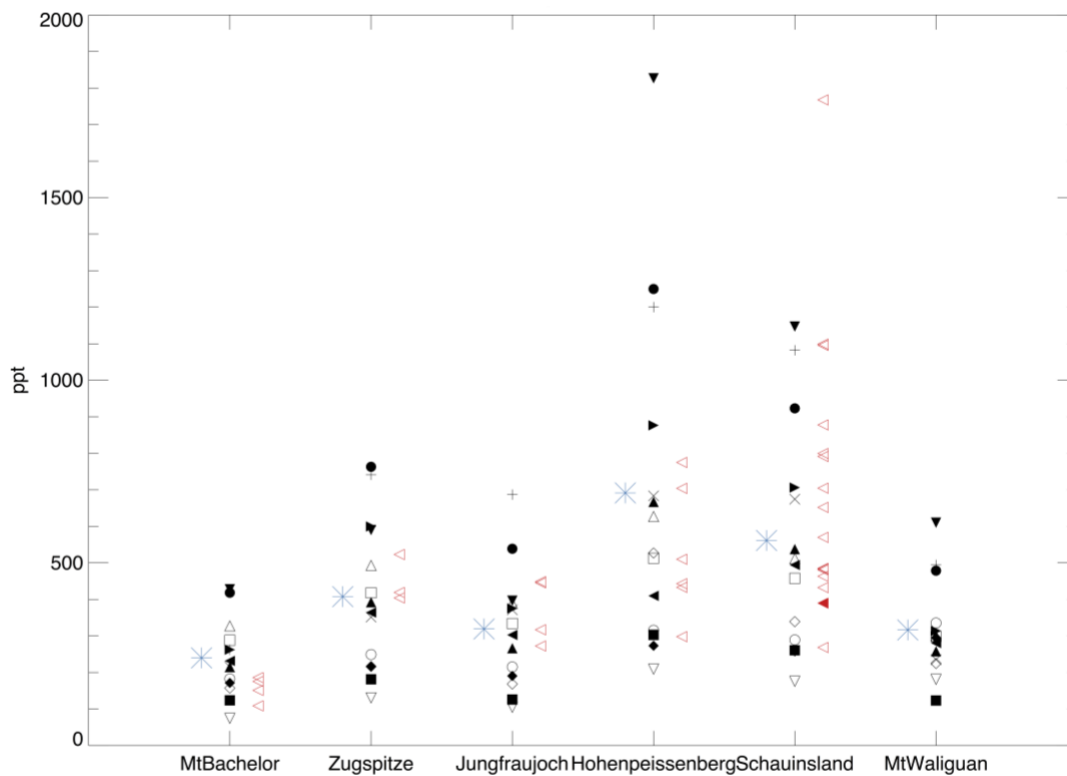
805 **Figure 1: Multi-model monthly mean total PAN mixing ratios (black circles and solid lines) at Mt. Bachelor**
 806 **(left) and Jungfraujoch (right). We take the difference between the base simulation (SR1) and one in which**
 807 **emissions are decreased by 20% and then multiply the difference by 5 to estimate a 100% contribution**
 808 **associated with anthropogenic precursor emissions from Europe (green), North America (red), East Asia (blue).**
 809 **The sum of the anthropogenic contribution from these three regions is shown (dashed black) for comparison**
 810 **with total simulated PAN.**

811



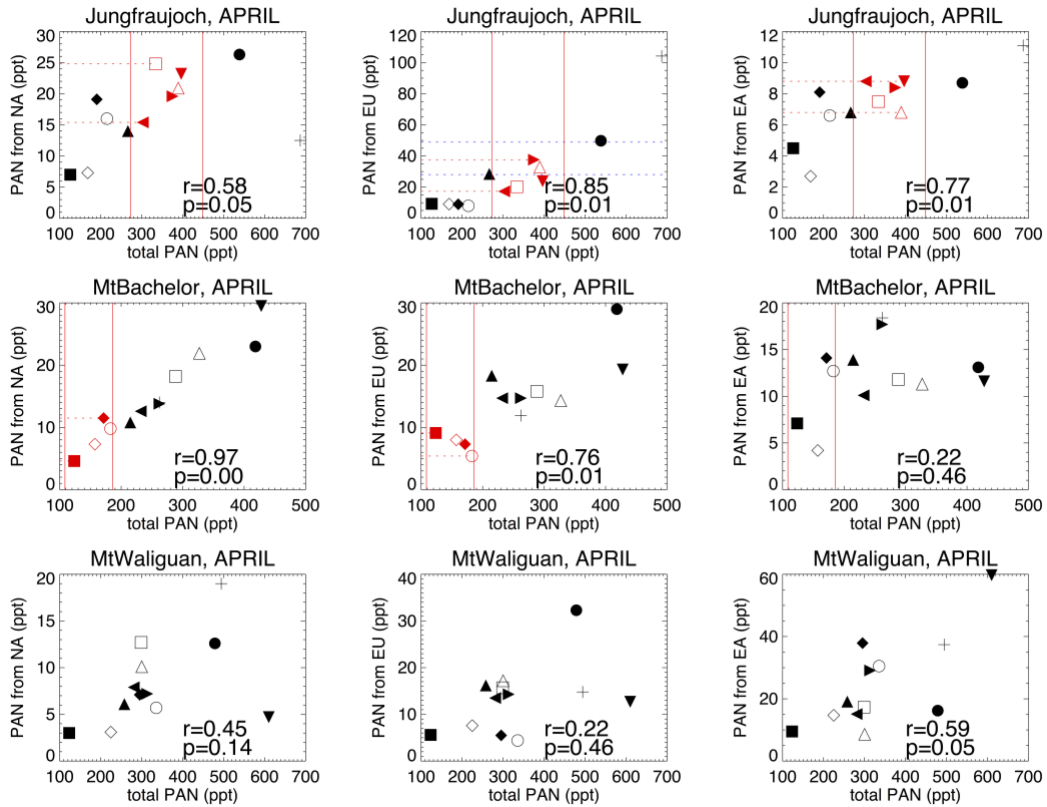
812

813 **Figure 2: Multi-model ensemble (n=14; Table 1) average PAN mixing ratios (ppt; left panels) and relative**
 814 **standard deviation (the absolute standard deviation across the models divided by the ensemble mean; right**
 815 **panels) at 650 hPa in April; relative standard deviations are masked out (white) for regions where multi-model**
 816 **mean PAN falls below 100 ppt. The models were sampled at 650 hPa by vertically interpolating between the**
 817 **bounding grid cells and then re-gridded horizontally to a common 1°x1° grid. White lines denote the HTAP1**
 818 **source regions: North America (NA), Europe and North Africa (EU), and East Asia (EA) from left to right.**
 819 **White circles indicate the five mountain sites with multi-year PAN observations used in our analysis (note:**
 820 **Zugspitze and Hohenpeissenberg are too close to differentiate on the map; see Table 3). Mount Waliguan in**
 821 **Asia, where we lack multi-year measurements but conduct model analysis, is denoted by the white square.**



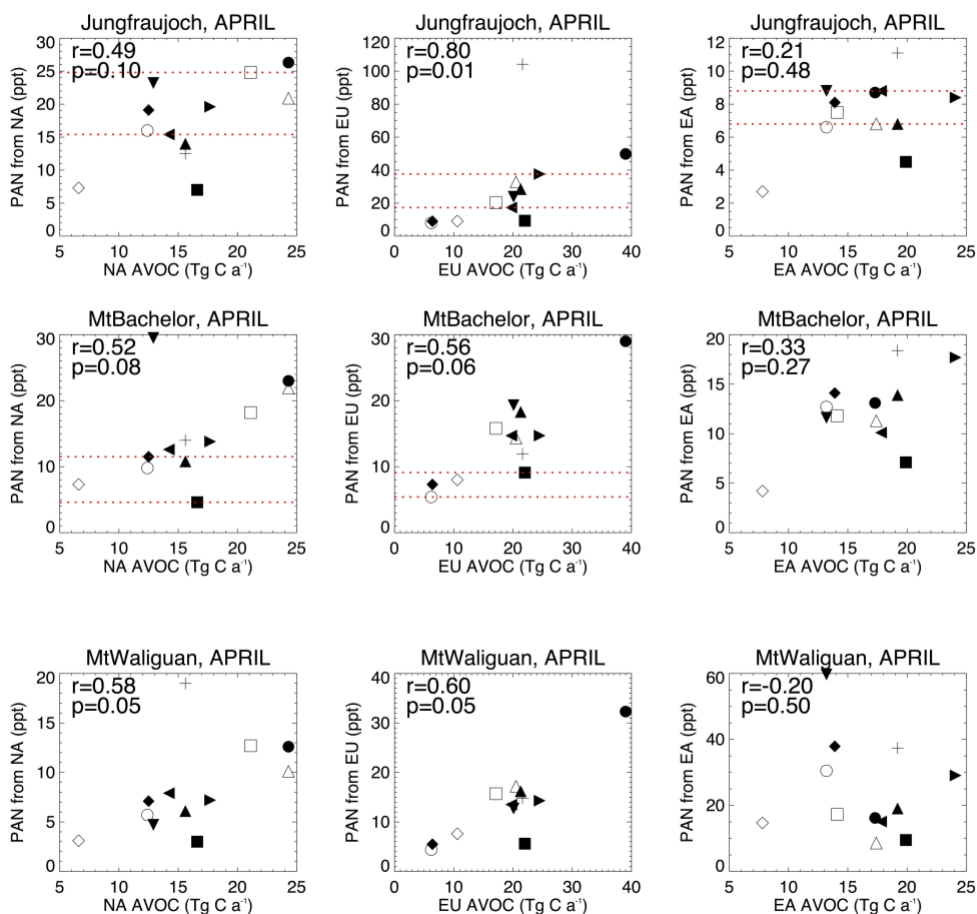
822

823 **Figure 3. April mean PAN abundances (ppt) simulated (black symbols, one per model as defined in Table 1;**
 824 **blue asterisk shows multi-model mean) and measured at northern mid-latitude mountaintop sites (red sideways**
 825 **triangles offset to the right of the model values; the year 2001 value, which corresponds to the meteorological**
 826 **year used by most of the models, at Schauinsland is filled).**



827

828 **Figure 4. Simulated total PAN versus source-receptor relationships (SRRs) at each of three northern mid-**
 829 **latitude sites. For Jungfrauoch and Mount Bachelor, vertical red lines bound the observed range in total PAN.**
 830 **For source-receptor pairs with significant correlations ($p \leq 0.05$), models falling within the observed range**
 831 **(across years) are colored red, and horizontal red dashed lines extend to the ordinate, representing the emergent**
 832 **constraint (narrower range resulting from selecting only those models falling in the observed range of total**
 833 **PAN). At Jungfrauoch, the range (across years) in PAN attributed to the EU source region by back-trajectory**
 834 **analysis (Pandey Deolal, 2013) is indicated by horizontal dashed blue lines. Individual models are denoted by**
 835 **the symbols defined in Table 1.**



837

838 **Figure 5: SRRs diagnosed as the difference between the SR1 and SR6xx simulations in Table 1 for PAN (ppt)**
 839 **Jungfrauoch (top), Mount Bachelor (middle), and Mount Waliguan (bottom) in each HTAP1 model (see Table**
 840 **1 for symbol assigned to each model) versus the annual emission of anthropogenic VOC (AVOC; Tg C a⁻¹)**
 841 **within the NA (left), EU (middle) and EA (right) source regions. The Spearman rank correlation coefficient**
 842 **(more robust to outliers than the traditional Pearson coefficient) and associated p-value are shown in each panel.**
 843 **The horizontal red lines correspond to the values identified with the red symbols in Figure 4.**

844

845

846

847

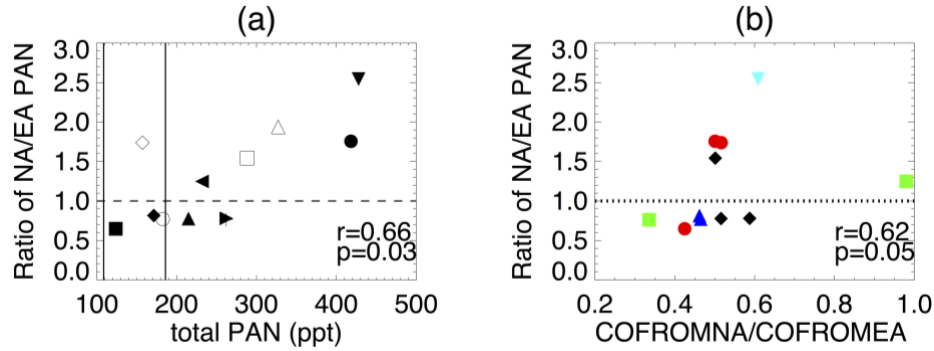
848

849

850

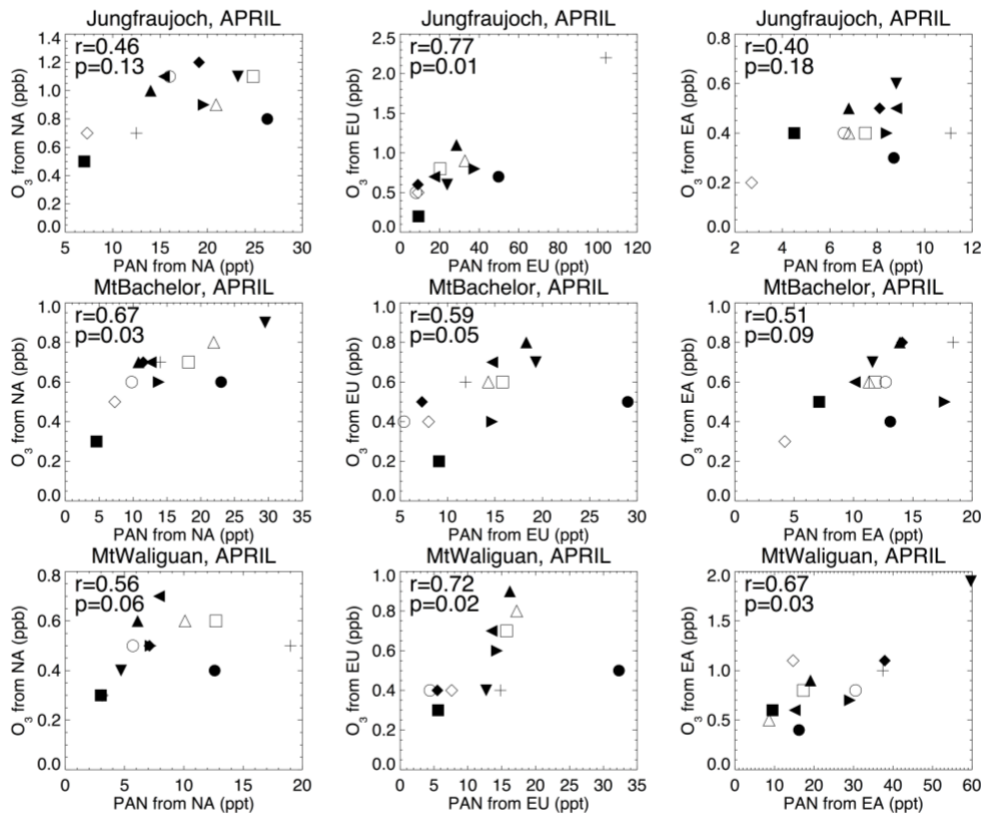
851

852



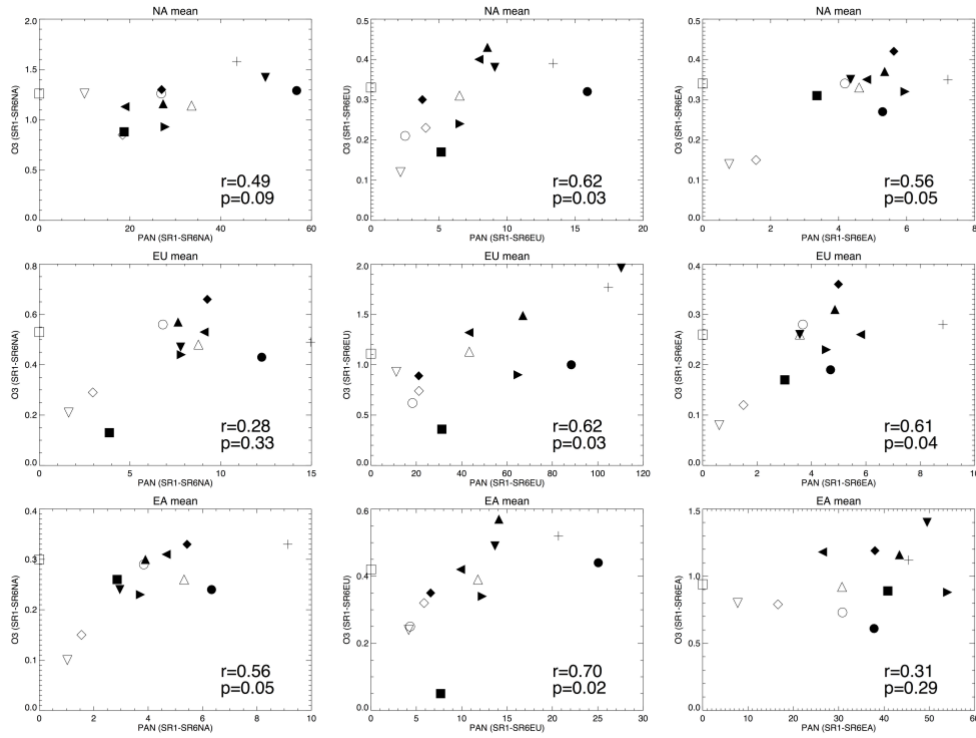
853

854 **Figure 6a:** Ratio of the PAN response to 20% emission reductions within NA versus EA plotted against (a) total
 855 PAN and (b) the ratio of idealized tracers of model transport emitted from NA versus EA
 856 (COfromNA/COfromEA; see Table 2) at Mount Bachelor as simulated by the HTAP1 models. Each symbol in
 857 (a) represents a model as defined in Table 1; the range of observed total PAN at Mount Bachelor is indicated by
 858 the black vertical lines. The colored symbols in (b) represent the meteorological fields used in the simulation:
 859 blue triangles for GEOS winds; red circles for NCEP; black diamonds for ECMWF; cyan upside-down triangles
 860 for CMC; green squares for general circulation models forced by observed sea surface temperatures and sea ice.
 861 Both panels show Spearman rank correlation coefficients and p-values, as well as a black dashed horizontal line
 862 at 1 to separate the models suggesting a higher NA influence (above) versus higher EA influence (below) on PAN
 863 SRRs.



864

865 **Figure 7:** SRRs for O₃ versus PAN at Jungfraujoch (top), Mount Bachelor (middle), and Mount Waliguan
 866 (bottom), obtained by subtracting the SR6XX from the SR1 simulations (Table 2) available from 12 models,
 867 where XX denotes the NA (left), EU (middle) or EA (right) source region. Each model thus contributes one point
 868 (symbols defined in Table 1) in each panel. Spearman (rank) correlation coefficient and p-values are also shown.



869

870 **Figure 8: SRRs for O₃ versus PAN in surface air over each of the HTAP1 northern mid-latitude continental**
 871 **regions: NA (top), EU (middle), and EA (bottom), obtained by subtracting the SR6XX from the SR1**
 872 **simulations, where XX denotes the NA (left), EU (middle) or EA (right) source region. Spearman (rank**
 873 **correlation coefficient and p-values are also shown. Symbols denote individual models as defined in Table 1.**
 874 **STOC-HadAM3-v01 is excluded here as an outlier that artificially raised the correlation significance.**